Atmospheric Environment 337 (2024) 120778

Contents lists available at ScienceDirect

Atmospheric Environment

journal homepage: www.elsevier.com/locate/atmosenv

Effects of NO_x and NH_3 on the secondary organic aerosol formation from α-pinene photooxidation

Yingqi Zhao [a,b], Zhaoyan Zhang [a,b], Ya Zhao [a], Chong Wang [c,d], Hua Xie [a], Jiayue Yang [a], Weiqing Zhang [a], Guorong Wu [a], Gang Li [a,**], Ling Jiang [a,e,*], Xueming Yang [a,c,e,f]

[a] State Key Laboratory of Molecular Reaction Dynamics and Dalian Coherent Light Source, Dalian Institute of Chemical Physics, Chinese Academy of Sciences, 457 Zhongshan Road, Dalian, 116023, China
[b] University of Chinese Academy of Sciences, 19A Yuquan Road, Beijing, 100049, China
[c] Institute of Advanced Science Facilities, Shenzhen, 518107, China
[d] Department of Chemical Physics, University of Science and Technology of China, Hefei, 230026, China
[e] Hefei National Laboratory, Hefei, 230088, China
[f] Department of Chemistry and Guangdong Provincial Key Laboratory of Catalytic Chemistry, Southern University of Science and Technology, Shenzhen, 518055, China

HIGHLIGHTS

- This study investigates the atmospheric components affected by the anthropogenic-biogenic interactions.
- The suppression effect of NO and NO_2 on the α-pinene photooxidation shows monotonous and parabolic trends, respectively.
- NH_3 enhances the number concentrations of SOA from the α-pinene + NO_x photooxidation by reacting with organic acids.
- A series of newly-observed compounds advance understanding of atmospheric components.

GRAPHICAL ABSTRACT

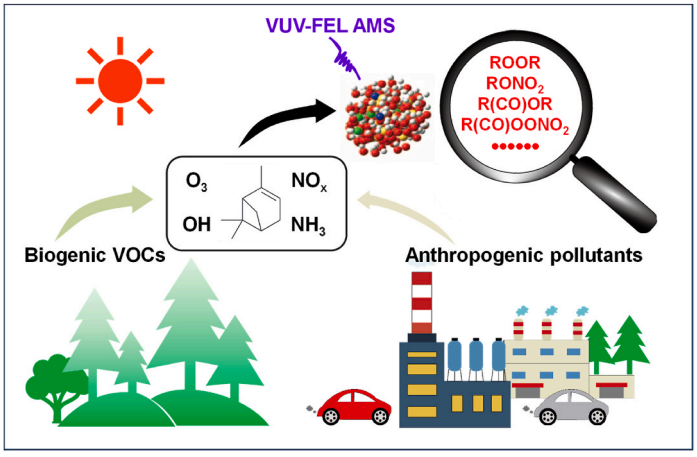

ARTICLE INFO

Keywords:
Anthropogenic–biogenic interactions
Secondary organic aerosol
Volatile organic compound
Photooxidation mechanism
α-pinene

ABSTRACT

Understanding the effects of mixed anthropogenic pollutants on the photooxidation of volatile organic compounds (VOCs) is essential for unraveling the formation pathways of secondary organic aerosols (SOA). Yet, it remains a highly challenging experimental target owing to the complexities in the precise measurement of molecular compositions of products and number/mass concentrations of particles as a function of pollutant concentration in the ambient atmosphere. Here, a series of well-defined chamber experiments were performed to

* Corresponding author. State Key Laboratory of Molecular Reaction Dynamics and Dalian Coherent Light Source, Dalian Institute of Chemical Physics, Chinese Academy of Sciences, 457 Zhongshan Road, Dalian, 116023, China.
** Corresponding author.
E-mail addresses: gli@dicp.ac.cn (G. Li), ljiang@dicp.ac.cn (L. Jiang).

https://doi.org/10.1016/j.atmosenv.2024.120778
Received 15 March 2024; Received in revised form 5 August 2024; Accepted 22 August 2024
Available online 23 August 2024

explore the effects of NO_x and NH_3 on the SOA formation from photooxidation of the most abundant monoterpene, α-pinene. The results indicate that the suppression effect of NO and NO_2 on the α-pinene photooxidation shows monotonous and parabolic trends, respectively. The presence of NH_3 enhances particle number concentrations during the α-pinene + NO_x photooxidation by participating in reactions with organic acids. New compounds, including organic peroxides, esters, organic nitrates, and peroxyacyl nitrates, are observed at molecular weight (MW) = 166, 173, 217, 231, 280, 282, 304, and 410 through threshold photoionization making use of a recently constructed vacuum ultraviolet free electron laser in positive ion mode. The molecular structures and formation paths of these species are speculated, which advance the category of VOC oxidation products. Our study provides significant understanding of the influence of NO_x and NH_3 on the VOC photooxidation, which can be utilized to establish predictive SOA formation networks and to improve atmospheric models.

1. Introduction

Secondary organic aerosol (SOA) adversely affects atmospheric visibility, climate, and human health (Huang et al., 2014; Jimenez et al., 2009). Among the volatile organic compounds (VOCs), biogenic VOCs (BVOCs) with relatively high emission rates are crucial precursors of SOA globally (Sindelarova et al., 2014). Experimental studies have indicated that the interactions between the compounds released by anthropogenic activities and BVOCs in the atmosphere lead to high concentrations of SOA (Yee et al., 2020). Given the significance of anthropogenic−biogenic interactions, the current challenge in model studies is to accurately simulate the complex atmospheric conditions and to fully elucidate the mechanisms of SOA formation (Boyd et al., 2015).

Monoterpene ($C_{10}H_{16}$) with estimated emissions of 100 Tg/year accounts for approximately 11% of BVOCs emissions (Hoffmann et al., 1997). The reactions of monoterpene with atmospheric oxidants readily occur, resulting the promotion of new particle formation (NPF) (Pye et al., 2010). Specifically, acting as the key precursor for the formation of SOA globally, α-pinene accounts for approximately 34% of the total monoterpene content (Guenther et al., 2012). In recent decades, intensive investigations have been conducted on the α-pinene-derived SOA, by which molecular structures of monomers and oligomers might be retrieved and their potential formation pathways could be observed (Berndt et al., 2016; Kenseth et al., 2023; Zhang et al., 2015; Zhao et al., 2021).

NO_x is primarily emitted from industrial processes and fuel combustion (Ohara et al., 2007). Elucidating the effects of NO_x on the oxidation processes of BVOCs provides important insights into the mechanisms of atmospheric SOA formation (Draper et al., 2015; Sarrafzadeh et al., 2016). Pioneering experiments of the α-pinene + NO_x photooxidation have predominantly highlighted the suppression effect of NO_x (Wildt et al., 2014), analyzed the compositions of particulate-phase products (Park et al., 2017), and explored potential formation pathways of highly oxygenated organic molecules (HOMs). The α-pinene ozonolysis appeared to govern largely the primary nature of SOA forming in α-pinene photooxidation under high relative humidity conditions (Yu et al., 2008). Increasing the concentrations of NO_x ($[NO_x]$) not only suppresses the NPF but also decreases the rate of SOA production (Eddingsaas et al., 2012). It was observed that during the process of high NO_x photooxidation, the SOA predominantly contained nitrogen-containing compounds (Park et al., 2017). These studies yielded significant outcomes for understanding the individual influence of NO_x on the α-pinene photooxidation processes.

Over the past century, NH_3 has been identified as the primary alkaline anthropogenic pollutant resulting from agricultural and industrial activities (Erisman, 2021). With the control of vehicular NO_x in recent years, the NH_3 concentrations have been increasing (Reche et al., 2022). Due to the complex reaction mechanisms of NH_3 with other atmospheric compounds, lots of research have been carried out to examine the effect of NH_3 on NPF (Gu et al., 2021). The study on the effect of NH_3 on the SOA formation from the α-pinene/ozone oxidation system indicates that NH_3 can interact with gas-phase organic acids to form condensable salts, resulting in the enhancement of SOA formation (Na et al., 2007). The coefficients of NH_3 uptake onto SOA were found to be positively correlated with particle acidity (Liu et al., 2015). The SOA yield for dark α-pinene ozonolysis and photooxidation in the presence of NH_3 was found to be higher as compared to the absence of NH_3 (Bin Babar et al., 2017). In the α-pinene + NH_3 + NO_x photooxidation, the NH_3–SOA interaction can induce the changes of particle size, aerosol mass, and chemical composition; furthermore, the reactions of organic acids with NH_3 in the low NO_x conditions would be much earlier than those in the high NO_x conditions (Hao et al., 2020).

Chamber experiments have been carried out to investigate the impacts of low- and high-NO_x on the SOA formation (Eddingsaas et al., 2012; Pullinen et al., 2020; Sarrafzadeh et al., 2016; Stirnweis et al., 2017). However, the individual role of NO and NO_2 in the HOMs formation would be different. For instance, recent research has shown that pure NO_2 suppressed the production of HOMs with mixture of α-pinene and Δ^3-carene, whereas NO exhibited a trend of initially increasing and then decreasing in the production of HOMs (Nie et al., 2023). Here, we explored the individual and joint effects of a specific NO_x component (NO, NO_2) and NH_3 on the molecular compositions of products and number/mass concentrations of particles formed from the α-pinene photooxidation. The molecular structures and formation pathways for newly-observed organic peroxides (i.e., esters, organic nitrates, and peroxyacyl nitrates (PAN)) were proposed via a combination of experimental results and quantum chemical calculations. Our present results offer comprehensive insights into the complex interactions between α-pinene, NO_x, and NH_3 during the daytime, illuminating the underlying mechanisms involved in the formation of SOA influenced by both anthropogenic and biogenic factors.

2. Experimental and theoretical methods

The experimental instrument mainly consists of a 2 m^3 smog chamber system and a photoionization mass spectrometer. A comprehensive description of experimental details could be found in a prior study (Zang et al., 2024) and in the Supporting Information (SI). A concise overview is presented here. The temperature of smog chamber was kept constantly at 298 ± 0.5 K. Relative humidity of smog chamber was less than 3%. Before experiments, the smog chamber was cleaned using the automatic cleaning mode, wherein the smog chamber was flushed through zero air for 8 h to remove any residual pollutants. α-Pinene (98.0%, Aladdin) was injected into the reactor through the inlet. Subsequently, known amounts of NO, NO_2, and NH_3 (with NO_2 and NH_3 balanced at 500 ppm in N_2, and NO balanced at 0.5000% in N_2) were introduced into the reactor through separately calibrated cylinders using flow controllers. All reactions were performed under conditions without seed aerosol.

The NO_x concentrations were monitored by Model 42i analyzer. Initial concentrations of NH_3 ($[NH_3]_0$) were determined by taking into account the volume of the reactor and the controlled injection amount. The O_3 concentrations were monitored using Model 49i analyzer. The VOC concentrations were monitored using a proton transfer reaction-mass spectrometer (PTR-QMS 3500, East & West Analytical Instruments, China). The α-pinene concentrations ($[\alpha$-pinene$]$) were determined by its fragment ions (molecular weight (MW) = 137 and 81). A scanning mobility particle sizer (SMPS 3938NL76) was used to

measure the size distributions, number concentrations, and mass concentrations of particles.

The full particles were seamlessly transferred from the smog chamber via a 1-m-long silicone tubing (inner diameter: 6.35 mm; length: 1000 mm) and aerodynamic lenses and deposited onto a copper rod (diameter: 8 mm) mounted in a time-of-flight mass spectrometer (TOF-MS) chamber. The deposited particles were vaporized by using a cartridge heater, ionized by vacuum ultraviolet free electron laser (VUV-FEL), and detected by TOF-MS in positive ion mode. Our TOF-MS has been calibrated by a series of standard organic compounds (i.e., vanillin, 1-pentadecanol, n-Eicosane, etc.). The comparison of mass spectra of heater ON and OFF indicated that the ionization of gas-phase products had a negligible interference on the ionization of particles. The threshold photoionization of molecule was achieved by using the tunable VUV-FEL to lose an electron to produce a molecular ion M^+. The positions of mass spectral peaks detected in this work denote the MW values. Our self-designed aerosol TOF-MS is able to detect the main size distributions of particles, ranging from 30 to 2500 nm and detect particle-phase products in real-time. Various experimental conditions (e.g., VUV-FEL wavelength and pulse energy, [α-pinene], [NO], [NO_2], and [NH_3]) were tuned to acquire optimal experimental conditions. In order to optimize experimental conditions, the advantages of using a tunable VUV-FEL and high pulse energy were utilized to measure the threshold photoionization mass spectra of neutral compounds. Because different aerosol components may have different ionization potentials, the use of different VUV-FEL wavelength (photon energy) helps to achieve threshold ionization and to reduce the fragments. During the experimental optimization process, the VUV-FEL pulse energy dependence of mass spectral signal was assessed to prevent photoionization saturation. As evidenced by our previous research (Zhang et al., 2024), the fragmentation and reactions with threshold photoionization by using an appropriate VUV-FEL wavelength and pulse energy are negligible. Given the high cost of machine time for VUV-FEL beamlines and the shorter reaction time of α-pinene and NO_x at high concentrations compared to low concentrations, the compounds were analyzed using VUV-FEL photoionization mass spectrometer under conditions that exceed those typically encountered in the natural atmosphere.

The wall loss of aerosol was corrected using established methodologies as described in the literature (Pathak et al., 2007). It was reported that the density of α-pinene-drived aerosols was 1.32 g/cm^3 (Ng et al., 2007). In this work, the density of α-pinene-drived aerosols was assumed to be 1.3 g/cm^3 for the calculation of the particle mass concentration based on the volume concentration measured by SMPS. The SOA yield was determined by the ratio of the corrected particle mass concentrations (ΔM, μg/m^3) to the comsumption of α-pinene (Δ[α-pinene], μg/m^3) in the reaction. Representatively, the temporal profiles for wall-loss corrected and uncorrected particle number concentration and particle mass concentration in the 350 ppb α-pinene +59 ppb NO experiment are shown in Fig. S1 of Supplementary Material, indicating that the uncertainty of particle mass concentration was estimated to be <13.0%. When [α-pinene]$_0$ was 433 ppb, the wall loss rate for [α-pinene]$_0$ = 433 ppb was 8.9×10^{-6} s^{-1}, which were close to 10^{-6} s^{-1} (Fig. S2).

To understand the experimental results, quantum chemical calculations were performed at the ωB97XD/def2-TZVP level of theory (Frisch et al., 2016). Transition states (TSs) were optimized with the Berny algorithm and confirmed by the intrinsic reaction coordinate (IRC) calculations. Relative energies were corrected by the zero-point vibrational energy (ZPVE). Tables 1 and 2 list the experimental conditions. The effects of [α-pinene]$_0$/[NO_x]$_0$ ratios on the α-pinene photooxidation were investigated by varying [α-pinene]$_0$, [NO]$_0$, and [NO_2]$_0$. Due to the nature of chamber injection, the [α-pinene]$_0$ vary in the range of 310 ppb–388 ppb. As shown in Fig. S3, the deviation of average particle mass concentration between the 311 ppb α-pinene +200 ppb NO_2 and 370 ppb α-pinene +200 ppb NO_2 experiments is ~5%, indicating that a small variation of [α-pinene]$_0$ does not significantly affect the particle mass concentration.

Table 1
Experimental conditions of α-pinene + NO + NH_3 photooxidation reactions.

[α-pinene]$_0$ (ppb)	[NO]$_0$ (ppb)	[NH_3]$_0$ (ppb)	[α-pinene]$_0$ /[NO]$_0$	ΔROG (ppb)	ΔM (μg/m^3)
350	59	0	5.9	345	526
336	107	0	3.1	331	455
340	206	0	1.7	333	314
388	318	0	1.2	380	274
310	370	0	0.8	299	93
350	55	30	6.4	343	537
340	54	50	6.3	334	569
354	51	100	6.9	349	660
993	397	0	2.5	985	2122

[X]$_0$ stands for initial concentration of X, ΔROG for the amount of reacted organic gas, and ΔM for particle mass concentration.

Table 2
Experimental conditions of α-pinene + NO_2 + NH_3 photooxidation reactions.

[α-pinene]$_0$ (ppb)	[NO_2]$_0$ (ppb)	[NH_3]$_0$ (ppb)	[α-pinene]$_0$ /[NO_2]$_0$	ΔROG (ppb)	ΔM (μg/m^3)
333	59	0	5.6	327	424
335	98	0	3.4	330	672
338	151	0	2.2	335	868
370	200	0	1.9	365	547
311	200	0	1.6	302	517
340	287	0	1.2	330	410
327	63	30	5.2	321	445
323	52	50	6.2	316	657
348	57	100	6.1	340	794
580	112	0	5.2	559	810
588	289	0	2.0	574	1188
990	398	0	2.5	972	2307
987	411	100	2.4	977	2409
1312	405	0	3.2	1298	3330
1988	398	0	5.0	1960	5556

[X]$_0$ stands for initial concentration of X, ΔROG for the amount of reacted organic gas, and ΔM for particle mass concentration.

3. Results and discussion

3.1. Effects of NO_x and NH_3 on particle number concentrations, particle mass concentrations, and O_3 concentrations

The particle size distributions, particle number concentrations, particle mass concentrations, and O_3 concentrations based on the variation of [NO_x]$_0$, [α-pinene]$_0$, and [NH_3]$_0$ are shown in Figs. 1–4, S4, and S5, respectively. The temporal evolution of [NO_x], [O_3], and [α-pinene] under different conditions is shown in Figs. S7 and S8, respectively.

In the 350 ppb α-pinene +59 ppb NO photooxidation experiment (Fig. 1a$_1$), there is no NPF detected at the beginning of photooxidation. After 0.5 h, the number concentration of particles undergoes a rapid increase. As [NO]$_0$ increases from 59 ppb to 370 ppb, the moment of particle generation shifts later and the number concentration of SOA is gradually suppressed. In the 333 ppb α-pinene +59 ppb NO_2 photooxidation experiment (Fig. 1a$_2$), the particle size experiences a rapid increase within 1 h after nucleation and eventually stabilizes at a level. Upon increasing [NO_2]$_0$ from 59 to 151 ppb, NO_2 exhibits a gradual enhancement of particle number concentration. However, further elevating [NO_2]$_0$–287 ppb leads to a gradual suppression of particle number concentration. This non-linear variation of NO_2 effect on the particle number concentration as a function of [NO_2]$_0$ (Fig. 1a$_2$-e$_2$) is different from that of monotonically gradual variation of NO suppression effect (Fig. 1a$_1$-e$_1$).

The variation of particle mass concentrations and O_3 concentrations during the photooxidation experiments involving α-pinene with NO and α-pinene with NO_2 is shown in Fig. 2, respectively. It is observed that the changes in particle mass concentrations are almost synchronous with the accumulation of O_3 in time. This underlying relationship between

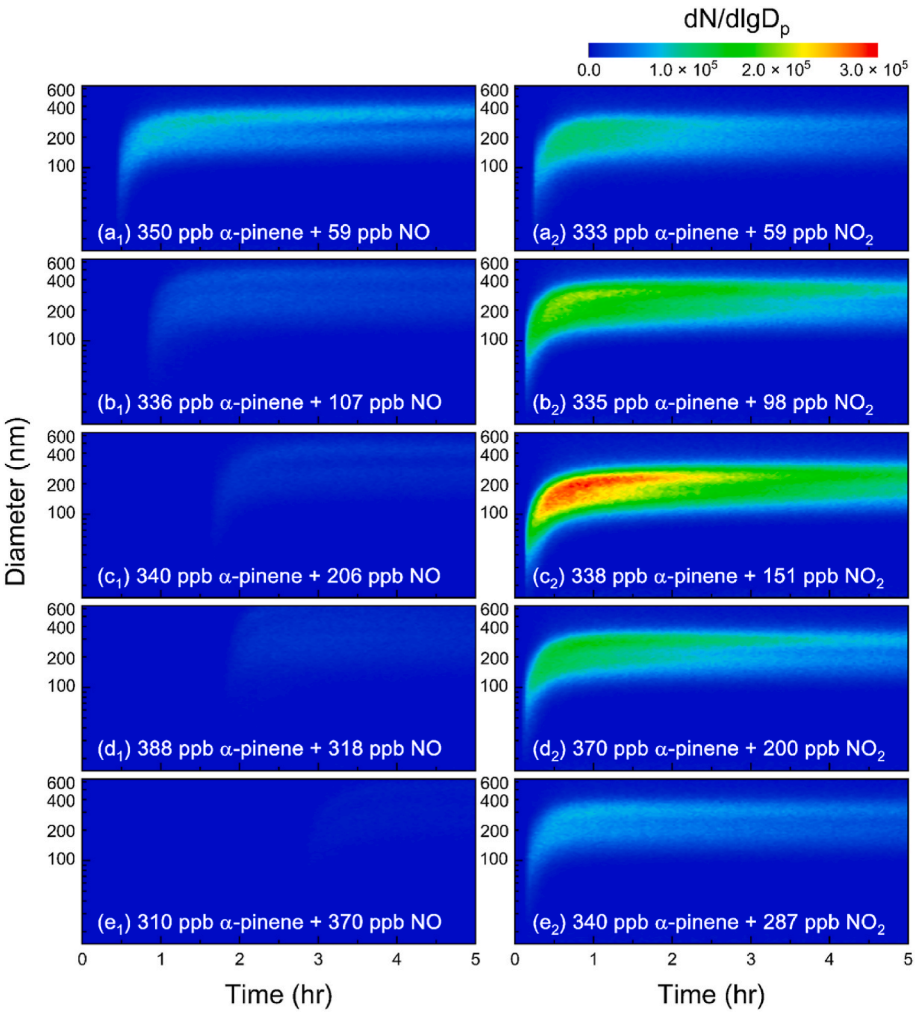

Fig. 1. Particle size distributions as a function of $[NO]_0$ and $[NO_2]_0$: (a_1) 350 ppb α-pinene + 59 ppb NO; (b_1) 336 ppb α-pinene + 107 ppb NO; (c_1) 340 ppb α-pinene + 206 ppb NO; (d_1) 388 ppb α-pinene + 318 ppb NO; (e_1) 310 ppb α-pinene + 370 ppb NO; (a_2) 333 ppb α-pinene + 59 ppb NO_2; (b_2) 335 ppb α-pinene + 98 ppb NO_2; (c_2) 338 ppb α-pinene + 151 ppb NO_2; (d_2) 370 ppb α-pinene + 200 ppb NO_2; (e_2) 340 ppb α-pinene + 287 ppb NO_2. Particle diameter is abbreviated as D_p. Normalized number size distribution is denoted by $dN/dlgD_p$.

particle mass concentration and O_3 indicates that O_3 may trigger the generation of particles. It is worth noting that O_3 is a notable byproduct of VOC chemical oxidation in the atmosphere, and its accumulation level can be used as an indicator of pollution status (Lelieveld et al., 2015). The accumulated amount of O_3 increases with $[NO]_0$ and $[NO_2]_0$, which indicates that $[NO_x]_0$ is a key factor in the generation of O_3. In the present photooxidation reactions of α-pinene with NO_2, we found that higher $[NO_2]_0$ could result in the more generation of O_3 (Fig. 2d). However, in the present photooxidation reactions of α-pinene with NO, the change of O_3 concentration is non-linear with $[NO]_0$ (Fig. 2c), which is reminiscent of the fact that the generation of O_3 in the real atmosphere may not be linear positively correlated with NO_x concentration (Liu and Shi, 2021). These findings suggest that under the conditions of severe NO_x pollution and abundant vegetation, long-term photooxidation reactions may accumulate more O_3, enhance the oxidative capacity of the corresponding troposphere and aggravate atmospheric pollution. In the α-pinene + NO_x photooxidation, the photolysis of NO_2 leads to a more direct production of oxidants (i.e., O_3 and OH) compared to the photolysis of NO. The reaction of NO with organic peroxy radicals (RO_2) forms the highly volatile organic nitrates and consequently suppresses the generation of low volatile species. This suggests that NO significantly suppresses the particle mass concentration, for which actual NO_x impact of depends on the composition and concentration of NO_x.

The $[VOC]/[NO_x]$ ratio has been shown to influence both the O_3 concentration and the SOA formation (Berezina et al., 2020; Reche et al., 2022). Accordingly, SOA yields and $[O_3]_{max}$ as a function of the $[\alpha\text{-pinene}]_0/[NO]_0$ and $[\alpha\text{-pinene}]_0/[NO_2]_0$ ratios are plot in Fig. 3. As $[NO]_0$ increases (Fig. 3a), the SOA yield continues to decline, which could be attributed to the fact that the increase of NO may directly induce competitive reactions, such as the formation of $RONO_2$. As $[NO]_0$ increases (Fig. 3c), $[O_3]_{max}$ first increases and then decreases. This shows with the photolysis of more $[NO]_0$, more O_3 is first produced and with the continuous increase of $[NO]_0$, the accumulation of O_3 may be suppressed due to the reaction between NO and O_3. As $[NO_2]_0$ increases (Fig. 3b), SOA yield first increases and then decreases. This suggests that in low NO_2 conditions, a slight increase in $[NO_2]_0$ can lead to higher levels of O_3 production via the photolysis of NO_2 (Fig. 3d), which enhances the oxidation of α-pinene, resulting in higher mass concentration and yield of SOA. Further increasing $[NO_2]_0$ may trigger some competing reactions, such as the formation of $RONO_2$. In this case, the increase of $[NO_2]_0$ may suppress the further generation of SOA and result in a decrease in SOA yield. As shown in Fig. S9, the SOA yield increases monotonically as $[\alpha\text{-pinene}]_0$ increases, whereas during the photooxidation process, the amount of accumulated O_3 decreases. This may be attributed to that more α-pinene is involved in the photooxidation reactions and consumes more O_3, causing a decrease in the O_3 concentration and an enhancement in the SOA formation. These experimental results have confirmed the importance of actual O_3

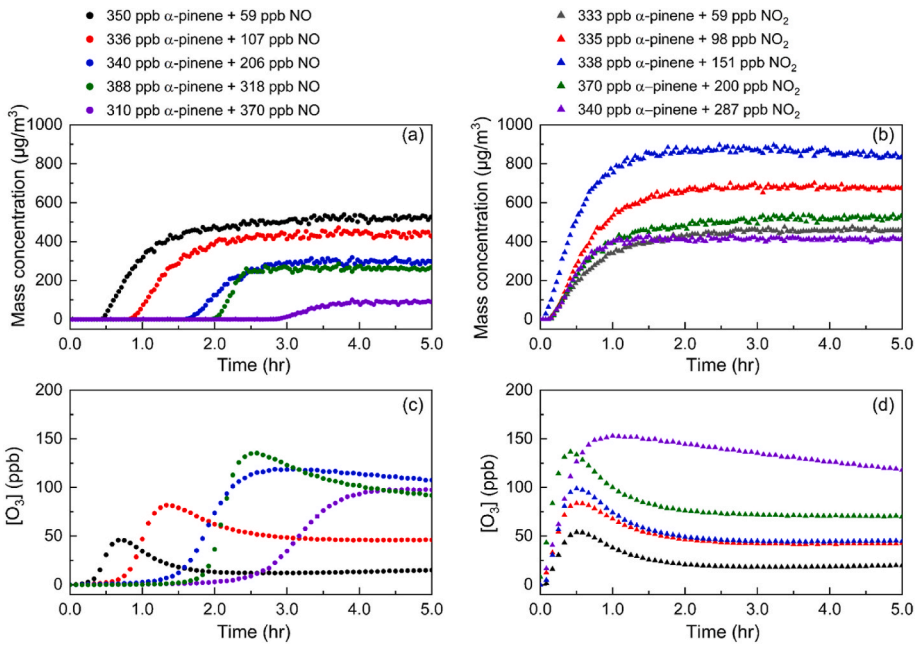

Fig. 2. Particle mass concentrations and O_3 concentrations at the experimental conditions with different $[NO_x]_0$. The dots and triangles represent the α-pinene + NO experiments (a and c) and α-pinene + NO_2 experiments (b and d), respectively.

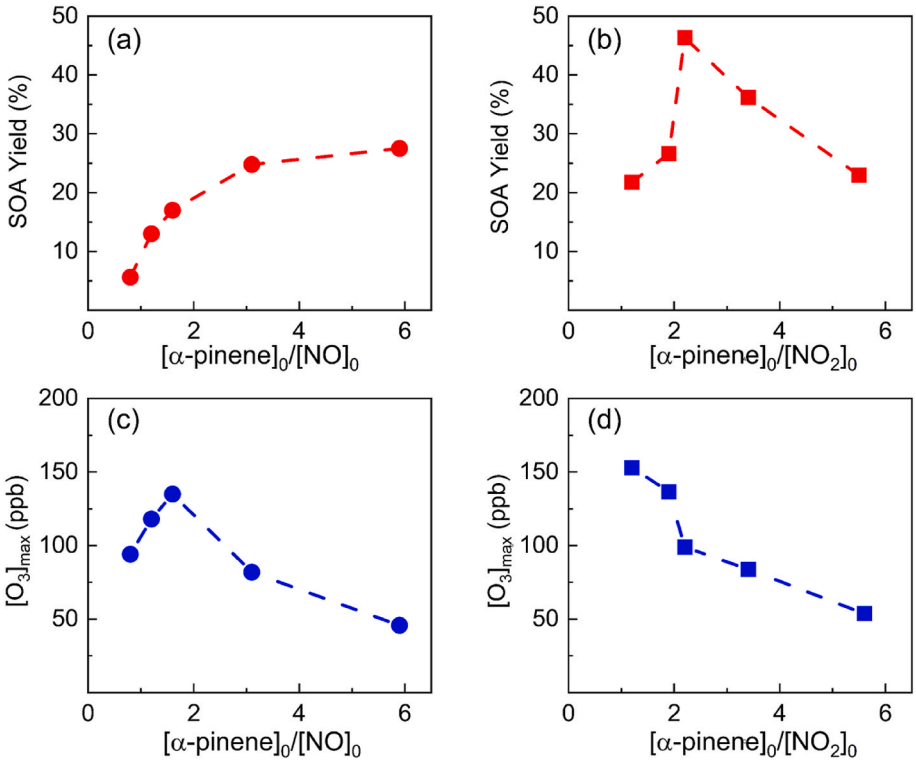

Fig. 3. SOA yields (a and b), and $[O_3]_{max}$ (c and d) as a function of $[\alpha\text{-pinene}]_0/[NO]_0$ and $[\alpha\text{-pinene}]_0/[NO_2]_0$.

concentration in the SOA formation and the influence of NO_x on the RO_2 chemistry complicates the relationship between O_3 and SOA formation.

Note that RO_2 have a significant contribution to a variety of atmospheric processes (Atkinson and Arey, 2003; Zhao et al., 2018). In the atmosphere, RO_2 can undergo unimolecular reactions to trigger the formation of HOM and bimolecular reactions with other compounds to form dimers and organic nitrates (Berndt et al., 2015; Hasan et al., 2020; Nihill et al., 2021; Perakyla et al., 2023; Tsiligiannis et al., 2019). The main mechanism discussed in this article for the formation of dimers (formed by reaction (R1, R2)), organic nitrates ($RONO_2$) (formed by reaction (R4)) and PAN (formed by reaction (R5)) through RO_2 reactions is given as follows:

$$RO_2 + R'O_2 \rightarrow ROOR' + O_2 \quad (R1)$$

$$R(CO)CH_2OO + R'O_2 \rightarrow R(CO)OR' + O_2 + HCHO \quad (R2)$$

$$RO_2 + NO \rightarrow RO + NO_2 \quad (R3)$$

$$RO_2 + NO \rightarrow RONO_2 \quad (R4)$$

$$R(CO)OO + NO_2 \rightarrow R(CO)OONO_2 \quad (R5)$$

For the α-pinene + NO experiments, as $[NO]_0$ increases, the formation rate of $RONO_2$ through the RO_2 + NO reaction (R4) also enhances, which suppresses the SOA formation. For the α-pinene + NO_2 experiments, due to the short lifetime of $ROONO_2$ formed by the RO_2 + NO_2 reaction, NO_2 has relatively less impact on the consumption of RO_2 than NO (Orlando and Tyndall, 2012; Rissanen, 2018). The increase of $[NO_2]_0$ may trigger the RCO(OO) + NO_2 reaction (R5), forming the R(CO)$OONO_2$ (PAN) product (Chan et al., 2010).

To explore the effects of NH_3 on the α-pinene + NO and α-pinene + NO_2 photooxidation, a series of experiments were performed by varying $[NH_3]_0$ (Fig. 4 and S6). In view of the implementation of policies such as increasingly strict NO_x emission control, the atmospheric NO_x content has been gradually reduced, but efforts to reduce NH_3 emissions are relatively unregulated (Gu et al., 2021; Hand et al., 2014; Hopke and Querol, 2022; Jia and Xu, 2020; Li et al., 2016; Ronald et al., 2017). In view of the effectiveness of the current NO_x emission reduction policy (Ronald et al., 2017), we mainly examined particle size distribution as a function of $[NH_3]_0$ under low-NO_x experimental conditions. The addition of NH_3 remarkably enhances the particle number concentration for α-pinene + NO photooxidation (Fig. 4a_1 and b_1), which is reminiscent of the NH_3 effect observed in the dark reaction between α-pinene and O_3 (Bin Babar et al., 2017). As $[NH_3]_0$ increases, the particle number concentration and particle mass concentration gradually increase, and the moment of nucleation event also becomes earlier (Fig. 4 and S6). Such enhancement effects of NH_3 on the α-pinene + NO photooxidation are also observed for those on the α-pinene + NO_2 photooxidation (Fig. 4a_2-d_2). These effects of NH_3 on the α-pinene + NO_x photooxidation are comparable to the effects on the toluene + NO_x photooxidation (Bao et al., 2021). Previous studies have shown that ammonium nitrate may be formed by the gas-phase reaction of nitric acid and ammonia in the presence of sufficient water vapors; water molecules are needed to stabilize the ion pair configuration of ammonium nitrate (Kumar et al., 2018; McCurdy et al., 2002; Tao, 1998); nitric acid and ammonia can nucleate directly to form ammonium nitrate particles at temperatures below −15 °C (Wang et al., 2020). Since our present experiments were conducted with RH < 3% at 25 °C, the ammonium nitrate may be not readily formed under such dry conditions. Considering that the vapor pressures of condensable salts from the gaseous reactions of organic acids and NH_3 were significantly lower than those of the corresponding acids (Paciga et al., 2014), the promotion effect of NH_3 may be due to the reactions of organic acids with NH_3 in the present experimental conditions.

The previous studies indicate that the suppressing effect of NO_x on SOA formation are ascribed to the formation of organic nitrates and the lowering of the OH level by NO_x (Eddingsaas et al., 2012; Ng et al., 2007; Pullinen et al., 2020; Sarrafzadeh et al., 2016; Stirnweis et al., 2017); higher concentrations of organic acids during α-pinene photooxidation could potentially correlate with higher ozonolysis reactivity (Friedman and Farmer, 2018; Hao et al., 2020). In this work, we found that as $[NO]_0$ increases, the particle number concentrations and particle mass concentrations are gradually suppressed, whereas $[O_3]_{max}$ first increases and then decreases; as $[NO_2]_0$ increases, the particle number concentrations and particle mass concentrations first increase and then decrease, whereas $[O_3]_{max}$ increases gradually. Notably, the presence of NH_3 enhances the particle number concentrations and particle mass concentrations for the photooxidation reactions of both α-pinene + NO and α-pinene + NO_2, which are analogous to the promotion effect of NH_3 in the SOA formation of the α-pinene + O_3 reactions (Bin Babar et al., 2017; Na et al., 2007) and to the contribution of NH_3 in the

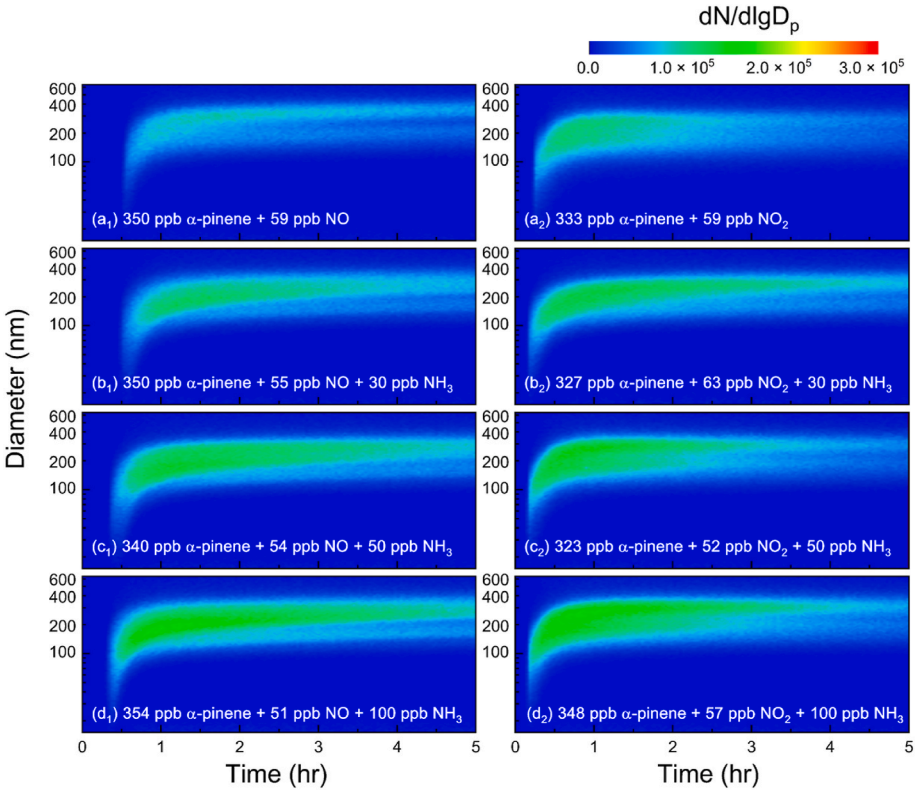

Fig. 4. Particle size distributions as a function of $[NH_3]_0$: (a_1) 350 ppb α-pinene + 59 ppb NO; (b_1) 350 ppb α-pinene + 55 ppb NO + 30 ppb NH_3; (c_1) 340 ppb α-pinene + 54 ppb NO + 50 ppb NH_3; (d_1) 354 ppb α-pinene + 51 ppb NO + 100 ppb NH_3; (a_2) 333 ppb α-pinene + 59 ppb NO_2; (b_2) 327 ppb α-pinene + 63 ppb NO_2 + 30 ppb NH_3; (c_2) 323 ppb α-pinene + 52 ppb NO_2 + 50 ppb NH_3; (d_2) 348 ppb α-pinene + 57 ppb NO_2 + 100 ppb NH_3.

transformation of gas-phase organic acids to the particle-phase ammonium (Hao et al., 2020).

3.2. Mass spectrometry of α-pinene photooxidation

Fig. 5 illustrates the mass spectra of compounds formed from the 990 ppb α-pinene and 398 ppb NO_2 condition. Higher mass peak intensities appear to be higher at 125.0 nm. Changing the wavelength of VUV-FEL from 125.0 nm to 133.0 nm results in the disappearance of several peaks (Fig. 5c). As shown in Table S1, the mass peak intensities at 118.0 nm were significantly weaker than those at 125.0 nm (Fig. 5a and b). These results indicate that neutral compounds can be selectively photoionized by the tunable VUV-FEL, which helps to advance our understanding of complex atmospheric chemical reactions.

Based on the above results, the photoionization mass spectra were obtained by operating the wavelength of VUV-FEL at 125.0 nm under a range of different experimental concentrations and conditions (Fig. 6). The mass peak intensities show a notable enhancement with the experimental conditions changing from Fig. 6a to b. This indicates that the complete process of α-pinene photooxidation is facilitated with the increase of $[NO_2]_0$ in a small range, which aligns with the aforementioned increase in the particle number concentration and particle mass concentration (Figs. 1 and 2). The further increase in mass peak intensities as the experimental conditions from Fig. 6b to c is in line with the rise in both mass concentration and number concentration under higher $[\alpha\text{-pinene}]_0$ and $[NO_2]_0$ conditions (Fig. S4 and Table 2). Representatively, the VUV-FEL photoionization mass spectra of the compounds generated from the 993 ppb α-pinene +397 ppb NO and 990 ppb α-pinene +398 ppb NO_2 reactions are shown in Fig. S10. It can be found that the MW = 254 species was observed in the experiments of α-pinene + NO_2 (Fig. 6c) and α-pinene + NO_2 + NH_3 (Fig. 6d), but was weakly detected in the α-pinene + NO reaction system (Fig. S10a). The potential formula for MW = 254 is $C_{13}H_{18}O_5$, for which formation mechanisms are shown in Fig. S11. With the addition of NH_3, the mass peak intensities under condition (d) (Fig. 6d) are higher than those under condition (c) (Fig. 6c), which supports the promotional effect of

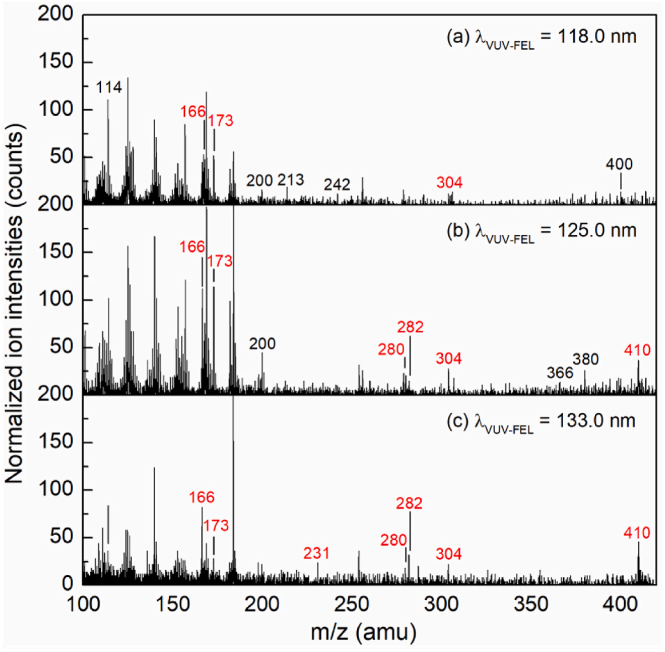

Fig. 5. Mass spectra of the compounds formed at the 990 ppb α-pinene and 398 ppb NO_2 condition measured with $\lambda_{VUV\text{-}FEL}$ = 118.0 nm (a), 125.0 nm (b), and 133.0 nm (c), respectively. The background has been subtracted. New compounds are marked with red.

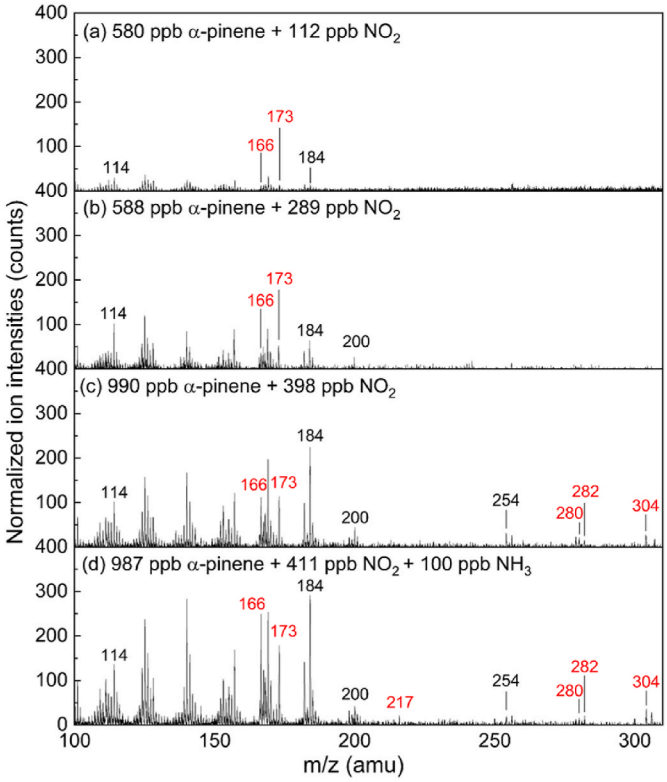

Fig. 6. Mass spectra of the compounds formed under different experimental conditions (a–d). The compounds were ionized by the VUV-FEL at 125.0 nm. The background has been subtracted. New compounds are marked with red.

NH_3 on the number concentration of particles (Fig. 4 and S5). In contrast with Fig. 6c, a small peak at MW = 217 is found in Fig. 6d, which may be resulted from the combined effect of NH_3 and NO_x.

The interactions between α-pinene, NO_x, and NH_3 influence the sources of O_3 and OH generation, ultimately affecting the formation of SOA in the complicated photooxidation cycle. The higher mass peak intensities with 100 < MW < 200 are attributed to higher concentrations of monomers (Fig. 6). With the increase of $[NO_2]_0$ (Fig. 6a and b), there is a concurrent increase in the O_3 and OH concentrations, which leads to a notable increase in the products of monomers generated from the O_3 and OH pathway. The peak intensities at MW = 166, 173, 200, 280, 282, and 304 in Fig. 6c are larger than those in Fig. 6b, as indicated by the data provided in Table S2. Meanwhile, the increase in $[\alpha\text{-pinene}]_0$ (Fig. 6b and c) leads to the formation of more RO_2, consequently enhancing the formation of monomeric and dimeric products. It is possible that the chemical compositions of aerosols generated in different initial conditions are different.

3.3. Characterization of the chemical constituents during α-pinene photooxidation

Under the current experimental conditions, O_3 and OH are the main oxidants, and the observed compounds at MW = 114, 184, and 200 are consistent with the primary products involved in the oxidation of α-pinene as determined in prior PTR-MS and ESI-MS measurements (Jia and Xu, 2020; Kahnt et al., 2018; Yu et al., 2008; Zang et al., 2022; Zhao et al., 2021). The OH radical is formed mainly by the reaction between α-pinene and O_3 (Chew and Atkinson, 1996), as well as the photolysis of O_3 (Simon et al., 2020). The OH radical serving as the main oxidant during the daytime reacts rapidly with VOCs through mechanisms such as addition to double bonds (OH-addition) and the hydrogen abstraction (H-abstraction) (Berndt et al., 2016; Zhang et al., 2019). With aforementioned contexts, possible molecular structures and reaction

processes of compounds with MW > 100 are analyzed by the combination of mass spectra and theoretical computations, but we do not rule out other possible structures and mechanisms. The structures of new species are summarized in Table S3 and their potential formation mechanisms are shown in Figs. 7–9, respectively. A schematic diagram of α-pinene photooxidation reaction is given in Scheme S1.

Fig. 7 shows the mechanisms for the generation of new compounds MW = 217, 231, and 304 initiated from the ozonolysis of α-pinene. These products are designated as $\mathbf{P_{O3}}$-$\boldsymbol{n}$ (n = 1–4) based on their respective molecular weights. The α-pinene + O_3 → $\mathbf{A_{O3}}$-**1** reaction is extremely exothermic with a predicted value of 60.2 kcal/mol, in agreement with the findings of earlier research on the α-pinene ozonolysis (Bagchi et al., 2020; Kristensen et al., 2017). The ring-opening reaction of $\mathbf{A_{O3}}$-**1** → $\mathbf{A_{O3}}$-**2** is exothermic with predicted value of 19.7 kcal/mol. Then, the isomerization of $\mathbf{A_{O3}}$-**2** forms $\mathbf{A_{O3}}$-**3** via an intramolecular hydrogen shift (H-shift), for which the exothermicity and barrier is predicted to be 15.6 and 14.7 kcal/mol, respectively. The $\mathbf{A_{O3}}$-**3** → $\mathbf{A_{O3}}$-**4** process is exothermic with a predicted value of 6.1 kcal/mol. Our computational results are consistent with the established understanding of the early stages of the α-pinene ozonolysis (Iyer et al., 2021). Ozone-derived RO_2, such as $\mathbf{A_{O3}}$-**4**, exhibits a suitable structure for the generation of ester accretion products following the dissociation of the RO radical (Perakyla et al., 2023). Thus, $\mathbf{P_{O3}}$-**4** (MW = 304) could be generated by the reaction of $\mathbf{A_{O3}}$-**4** with $\mathbf{A_{OH1}}$-**1**, releasing O_2 and HCHO, which process is extremely exothermic with a predicted value of 90.8 kcal/mol. $\mathbf{A_{O3}}$-**4** could also react with NO to produce $\mathbf{A_{O3}}$-**5** with a predicted exothermicity of 17.1 kcal/mol. The RO radical $\mathbf{A_{O3}}$-**5** releases HCHO and then reacts with O_2 to produce $\mathbf{A_{O3}}$-**6**, for which the exothermicity and barrier is predicted to be 25.3 and 4.6 kcal/mol, respectively. $\mathbf{A_{O3}}$-**6** reacts with NO_2 leading to the generation of $\mathbf{P_{O3}}$-**3** (MW = 231) with the predicted exothermicity of 20.6 kcal/mol. The $\mathbf{A_{O3}}$-**5** → $\mathbf{A_{O3}}$-**7** process is extremely exothermic with a predicted value of 76.6 kcal/mol, for which the mechanisms are detailed in Fig. S12. $\mathbf{A_{O3}}$-**7** reacts with HO_2 to form organic acid $\mathbf{P_{O3}}$-**1** (MW = 200) (Iinuma et al., 2004; Sekimoto et al., 2020) with the predicted exothermicity of 16.5 kcal/mol. Previous studies have shown that gas-phase organic acids contribute to the SOA formation by forming organic ammonium salts, in which energetic information of possible formation pathways remains elusive (Bin Babar et al., 2017; Hao et al., 2020; Liu et al., 2015; Na et al., 2007). Our calculation indicates that the organic acid $\mathbf{P_{O3}}$-**1** reacts with NH_3 to produce compound the organic ammonium salt $\mathbf{P_{O3}}$-**2** (MW = 217), which is exothermic with a predicted value of 12.7 kcal/mol.

The H-abstraction has been shown to be a pivotal mechanism in the formation of HOMs during the reaction of α-pinene with OH (Berndt et al., 2016). Accordingly, the possible mechanisms initiated from the H-abstraction reaction are proposed in Fig. 8, in which the newly-observed products MW = 166, 280, and 282 are labeled as $\mathbf{P_{OH1}}$-$\boldsymbol{n}$ (n = 1, 3, 4), respectively. $\mathbf{A_{OH1}}$-**1** reacts with NO to release NO_2 and then with O_2 to form $\mathbf{A_{OH1}}$-**2**, which process is extremely exothermic with a predicted value of 51.3 kcal/mol. $\mathbf{A_{OH1}}$-**2** reacts with NO to form $\mathbf{P_{OH1}}$-**2** (MW = 213), which is highly exothermic with a predicted value of 52.6 kcal/mol. The $\mathbf{A_{OH1}}$-**2** → $\mathbf{A_{OH1}}$-**3** process is also both thermodynamically exothermic and kinetically favorable. $\mathbf{A_{OH1}}$-**3** reacts with NO to form $\mathbf{A_{OH1}}$-**4**, which is exothermic, with the predicted exothermicity of 13.6 kcal/mol. $\mathbf{A_{OH1}}$-**4** releases CH_3COCH_3 and then reacts with O_2 to produce $\mathbf{A_{OH1}}$-**5**, for which the exothermicity and barrier is predicted to be 33.9 and 5.8 kcal/mol, respectively. The $\mathbf{A_{OH1}}$-**5** → $\mathbf{P_{OH1}}$-**4** (MW = 282) accretion reaction is exothermic with a predicted value of 38.2 kcal/mol.

The $\mathbf{A_{OH1}}$-**2** → $\mathbf{P_{OH1}}$-**1** (MW = 166) process is facile, for which the exothermicity and barrier is predicted to be 46.6 and 7.5 kcal/mol, respectively. The exothermicity and barrier of the $\mathbf{P_{OH1}}$-**1** → $\mathbf{A_{OH1}}$-**6** reaction is predicted to 59.7 and 2.0 kcal/mol, respectively. $\mathbf{A_{OH1}}$-**6** releases CH_3COCHO to form $\mathbf{A_{OH1}}$-**7**, for which the exothermicity and barrier is predicted to be 5.6 and 17.8 kcal/mol, respectively. The exothermicity and barrier of the $\mathbf{A_{OH1}}$-**7** → $\mathbf{A_{OH1}}$-**8** isomerization is predicted to 20.6 and 20.4 kcal/mol, respectively. $\mathbf{A_{OH1}}$-**8** undergoes an H-abstraction reaction to form $\mathbf{A_{OH1}}$-**9**, which is extremely exothermic with a predicted value of 100.6 kcal/mol. $\mathbf{A_{OH1}}$-**9** undergoes CO_2 release, followed by its reaction with O_2 to form $\mathbf{A_{OH1}}$-**11**, for which the exothermicity and barrier is predicted to be 46.4 and 2.7 kcal/mol, respectively. $\mathbf{A_{OH1}}$-**11** and $\mathbf{A_{OH1}}$-**2** undergoes accretion reaction leading to the generation of $\mathbf{P_{OH1}}$-**3** (MW = 280), which is exothermic with a predicted value of 34.5 kcal/mol.

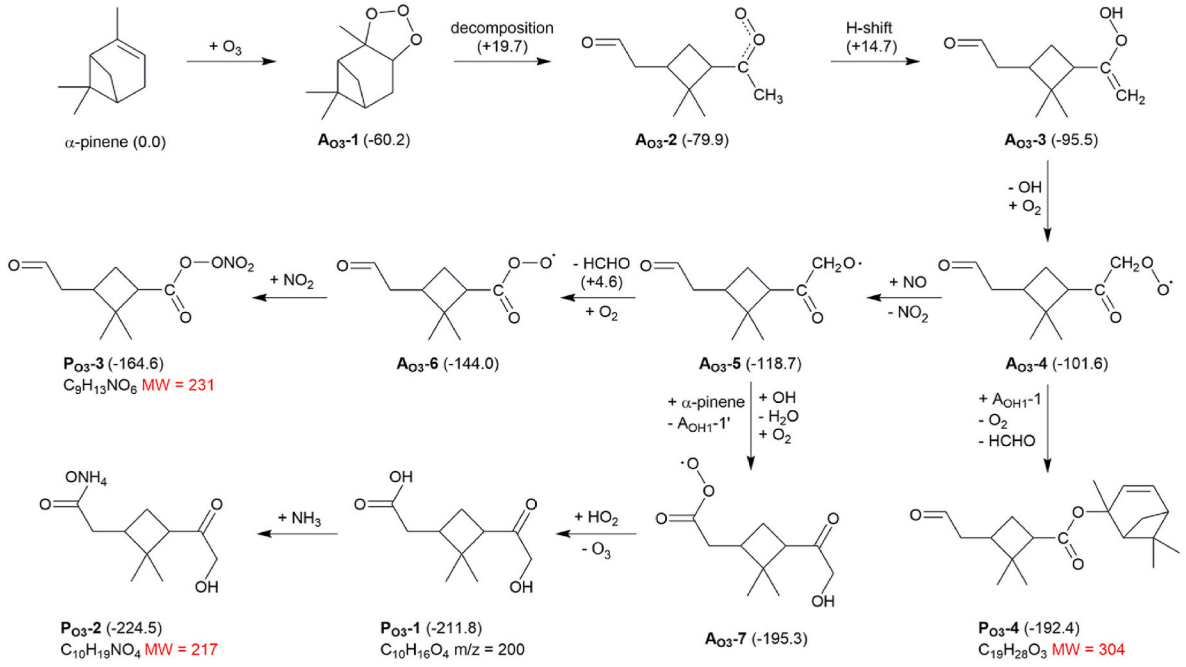

Fig. 7. Possible mechanisms for the formation of newly-observed species MW = 217, 231, and 304. Calculations were conducted at the ωB97XD/def2-TZVP level of theory. Energies relative to α-pinene are given in kcal/mol.

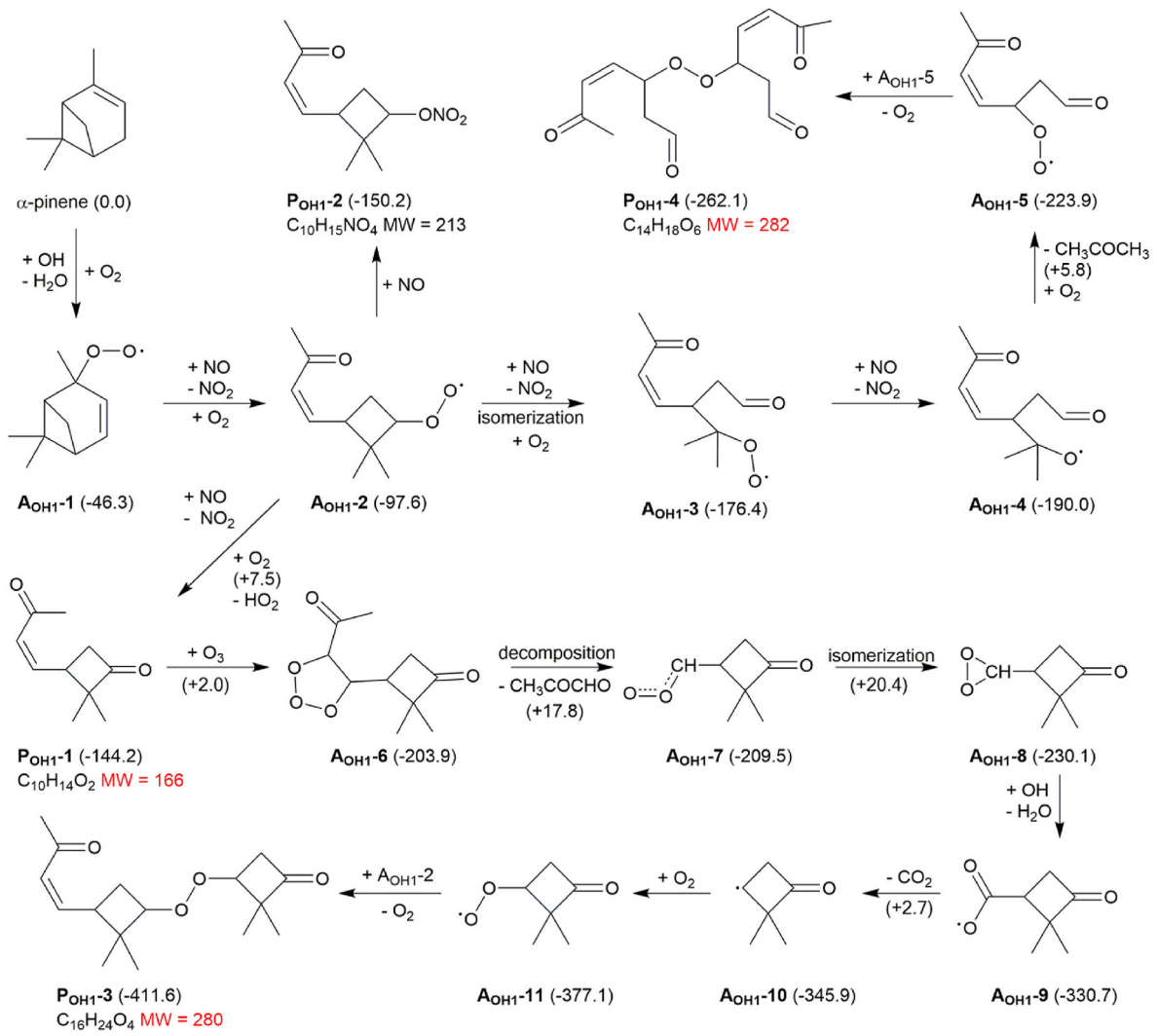

Fig. 8. Possible mechanisms for the formation of newly-observed species MW = 166, 280, and 282. Calculations were conducted at the ωB97XD/def2-TZVP level of theory. Energies relative to α-pinene are given in kcal/mol.

Fig. 9 analyzes the formation pathways of newly-observed species MW = 173 and 410 labeled as $\mathbf{P_{OH2}}$-***n*** (*n* = 1 and 2), stemmed from the OH-addition reaction. The α-pinene + OH → $\mathbf{A_{OH2}}$-**1** process is exothermic with a predicted value of 32.0 kcal/mol, consistent with the previous research (Berndt et al., 2016). The exothermicity and barrier of the $\mathbf{A_{OH2}}$-**1** → $\mathbf{A_{OH2}}$-**2** isomerization is predicted to be 7.7 and 14.6 kcal/mol, respectively. $\mathbf{A_{OH2}}$-**2** undergoes a reaction with O_2 to form $\mathbf{A_{OH2}}$-**3** with the predicted exothermicity of 14.1 kcal/mol. Similar to the $\mathbf{A_{OH1}}$-**3** → $\mathbf{A_{OH1}}$-**4** reaction (Fig. 8), the $\mathbf{A_{OH2}}$-**3** → $\mathbf{A_{OH2}}$-**4** reaction is exothermic with a predicted value of 26.9 kcal/mol and is also facile. $\mathbf{A_{OH2}}$-**4** releases CH_3COCH_3 to form $\mathbf{A_{OH2}}$-**5**, for which the exothermicity and barrier is predicted to be 3.2 and 16.6 kcal/mol, respectively. The $\mathbf{A_{OH2}}$-**5** + O_2 → $\mathbf{A_{OH2}}$-**6** reaction is estimated to be exothermic with a predicted value of 29.6 kcal/mol. The $\mathbf{A_{OH2}}$-**6** + NO → $\mathbf{P_{OH2}}$-**1** (MW = 173) reaction is highly exothermic with a predicted value of 51.4 kcal/mol. Similar to the α-pinene + O_3 → $\mathbf{A_{O3}}$-**2** process (Fig. 7), the $\mathbf{P_{OH2}}$-**1** → $\mathbf{A_{OH2}}$-**7** process is also facile, for which the exothermicity and barrier is predicted to be 66.4 and 20.5 kcal/mol, respectively (see Fig. S13 for details). The $\mathbf{A_{OH2}}$-**7** → $\mathbf{A_{OH2}}$-**8** reaction is exothermic with a predicted value of 20.6 kcal/mol. The $\mathbf{A_{OH2}}$-**8** → $\mathbf{P_{OH2}}$-**2** (MW = 410) accretion reaction is a highly exothermic process with the predicted exothermicity of 93.8 kcal/mol.

4. Conclusions

Currently, the concentrations of NO_x and NH_3 in the Earth's atmosphere have been steadily rising across multiple sources (Sobota et al., 2015; Sutton et al., 2011). We investigate the effects of NO_x and NH_3 on chemical compositions and particle number/mass concentrations through a series of laboratory experiments involving the α-pinene photooxidation. In contrast with previous studies (Nie et al., 2023), our results show that the suppression effect of NO and NO_2 on the α-pinene photooxidation shows monotonous and parabolic trends, respectively. Such difference may be due to variations in the concentrations of the specific component (NO and NO_2) and the types of VOC precursors. The multiple influences of NO_x and NH_3 pollutants on the α-pinene-derived particle formation (α-pinene + NO, α-pinene + NO_2, α-pinene + NO + NH_3, and α-pinene + NO_2 + NH_3) indicate that predicting atmospheric SOA formation based solely on the individual impacts of these pollutants (NO, NO_2, NH_3) may lead to biased results. By taking the advantage of high photoionization efficiency and a wide range of wavelength tunability of VUV-FEL, we have achieved in the detection of a series of new products (MW = 166, 173, 217, 231, 280, 282, 304 and 410) formed from the α-pinene photooxidation by NO_x and NH_3, which contributes to our comprehension of oxidation product categories.

The MW = 217 ($\mathbf{P_{O3}}$-**2**), 231 ($\mathbf{P_{O3}}$-**3**), and 304 ($\mathbf{P_{O3}}$-**4**) products are found to be generated via the oxidation channel of α-pinene ozonolysis;

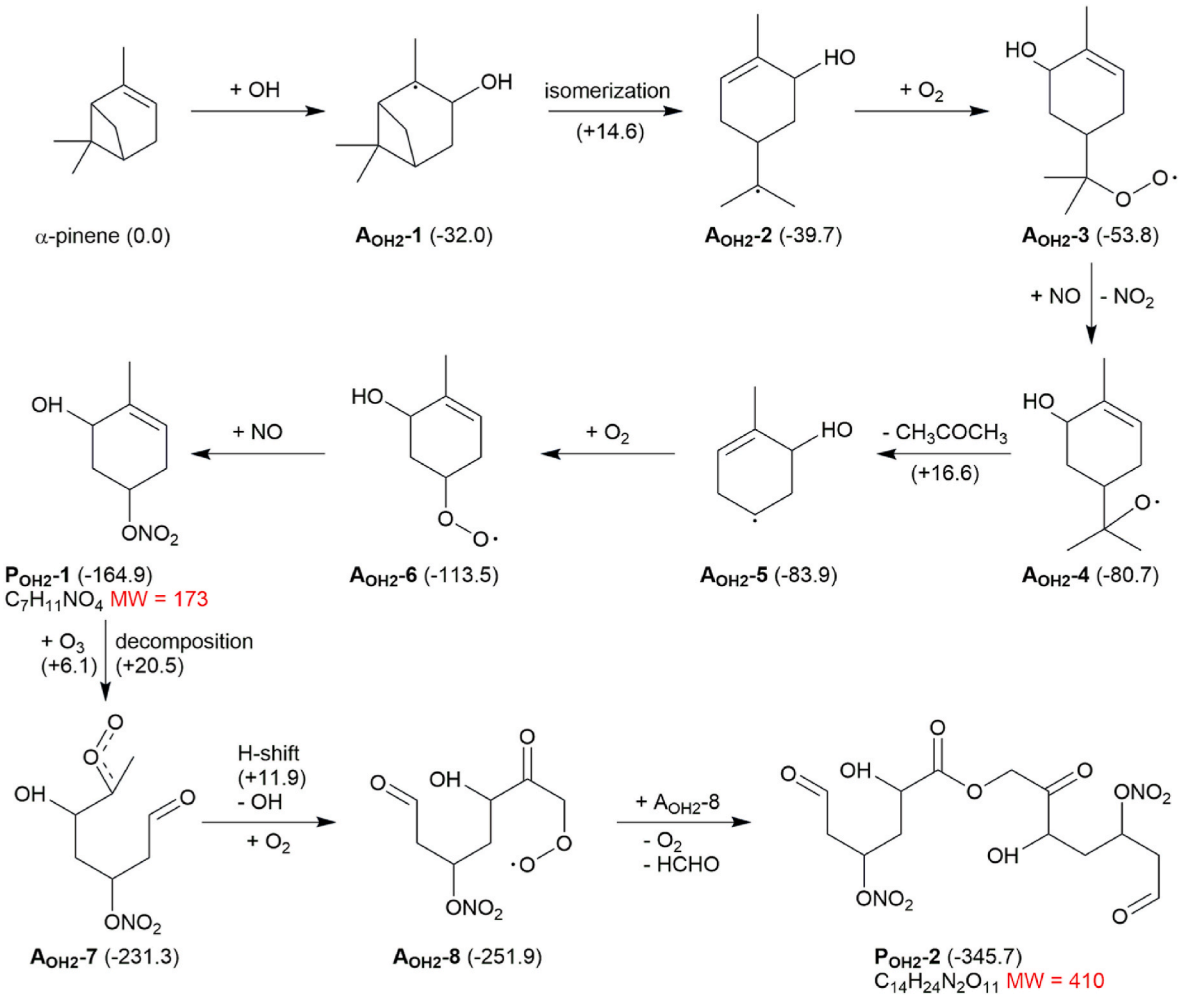

Fig. 9. Possible mechanisms for the formation of newly-observed species MW = 173 and 410. Calculations were conducted at the ωB97XD/def2-TZVP level of theory. Energies relative to α-pinene are given in kcal/mol.

the MW = 166 (**P_{OH1}-1**), 280 (**P_{OH1}-3**), and 282 (**P_{OH1}-4**) products are generated via the oxidation channel of H-abstraction product of α-pinene; the MW = 173 (**P_{OH2}-1**) and 410 (**P_{OH2}-2**) products are generated from the oxidation channel of OH-addition product of α-pinene. When both NO_x and NH_3 are present, the MW = 217 (**P_{O3}-2**) product is formed through the reaction of the MW = 200 (**P_{O3}-1**) with NH_3. These newly-observed species (i.e., dimeric accretion products, organic nitrates, and PAN) have been proposed in ambient particles and could function as enduring NO_x sinks with influence of NO_x and O_3 cycling (Berndt et al., 2018; Pye et al., 2015). Considering that NH_3 shows significant effects on the particle formation in different photochemical regimes have been confirmed (Bao et al., 2021; Bin Babar et al., 2017) and makes a direct contribution to SOA formation through acid-base reactions with organic compounds (Hao et al., 2020), we further proposed possible formation mechanisms and energetic information for the species generated in the experiments with the involemenet of NH_3. Our present findings provide strong evidence that direct involvement of NH_3 in the α-pinene + NO_x photooxidation leads to the SOA formation through the reaction of NH_3 with organic acids. As BVOCs are naturally emitted and difficult to be directly controlled, the effective regulation of NO_x emissions emerges as a viable strategy for mitigating aerosol pollution, complemented by the efficient control of NH_3 emissions. This study advances our understanding of how the interplay between anthropogenic and biogenic factors influences SOA formation in the neighborhood of emission origins.

CRediT authorship contribution statement

Yingqi Zhao: Writing – original draft, Methodology, Investigation, Formal analysis, Data curation, Conceptualization. **Zhaoyan Zhang:** Software, Investigation, Formal analysis, Data curation. **Ya Zhao:** Visualization, Investigation, Data curation. **Chong Wang:** Investigation, Formal analysis, Data curation. **Hua Xie:** Validation, Funding acquisition, Formal analysis. **Jiayue Yang:** Validation, Resources. **Weiqing Zhang:** Validation, Resources. **Guorong Wu:** Validation, Resources. **Gang Li:** Writing – review & editing, Writing – original draft, Visualization, Validation, Supervision, Project administration, Investigation, Funding acquisition, Conceptualization. **Ling Jiang:** Writing – review & editing, Writing – original draft, Visualization, Validation, Supervision, Project administration, Methodology, Investigation, Funding acquisition, Formal analysis, Data curation, Conceptualization. **Xueming Yang:** Validation, Resources, Project administration, Funding acquisition.

Declaration of competing interest

The authors declare the following financial interests/personal relationships which may be considered as potential competing interests:

Ling Jiang reports financial support was provided by National Natural Science Foundation of China.

Data availability

Data will be made available on request.

Acknowledgments

The authors gratefully acknowledge the Dalian Coherent Light Source (DCLS) and Specreation Co., Ltd. For support and assistance. This work was supported by the National Natural Science Foundation of China (Grant Nos. 22125303, 92361302, 92061203, 22103082, 22273101, 22288201, and 21327901), the National Key Research and Development Program of China (No. 2021YFA1400501), Innovation Program for Quantum Science and Technology (No. 2021ZD0303304), Dalian Institute of Chemical Physics (DICP I202437), Chinese Academy of Sciences (No. GJJSTD20220001), and International Partnership Program of CAS (121421KYSB20170012).

Appendix ASupplementary data

Supplementary data to this article can be found online at https://doi.org/10.1016/j.atmosenv.2024.120778.

References

Atkinson, R., Arey, J., 2003. Gas-phase tropospheric chemistry of biogenic volatile organic compounds: a review. Atmos. Environ. 37, 197–219.
Bagchi, A., Yu, Y., Huang, J.-H., Tsai, C.-C., Hu, W.-P., Wang, C.C., 2020. Evidence and evolution of Criegee intermediates, hydroperoxides and secondary organic aerosols formed via ozonolysis of α-pinene. Phys. Chem. Chem. Phys. 22 (12), 6528–6537.
Bao, Z., Xu, H., Li, K., Chen, L., Zhang, X., Wu, X., et al., 2021. Effects of NH_3 on secondary aerosol formation from toluene/NO_x photo-oxidation in different O_3 formation regimes. Atmos. Environ. 261, 118603.
Berezina, E., Moiseenko, K., Skorokhod, A., Pankratova, N.V., Belikov, I., Belousov, V., et al., 2020. Impact of VOCs and NO_x on ozone formation in Moscow. Atmosphere 11 (11), 1262.
Berndt, T., Scholz, W., Mentler, B., Fischer, L., Herrmann, H., Kulmala, M., et al., 2018. Accretion product formation from self-and cross-reactions of RO_2 radicals in the atmosphere. Angew. Chem. Int. Ed. 57 (14), 3820–3824.
Berndt, T., Richters, S., Kaethner, R., Voigtländer, J., Stratmann, F., Sipilä, M., et al., 2015. Gas-phase ozonolysis of cycloalkenes: formation of highly oxidized RO_2 radicals and their reactions with NO, NO_2, SO_2, and other RO_2 radicals. J. Phys. Chem. A 119 (41), 10336–10348.
Berndt, T., Richters, S., Jokinen, T., Hyttinen, N., Kurtén, T., Otkjær, R.V., et al., 2016. Hydroxyl radical-induced formation of highly oxidized organic compounds. Nat. Commun. 7 (1), 13677.
Bin Babar, Z., Park, J.-H., Lim, H.-J., 2017. Influence of NH_3 on secondary organic aerosols from the ozonolysis and photooxidation of α-pinene in a flow reactor. Atmos. Environ. 164, 71–84.
Boyd, C., Sanchez, J., Xu, L., Eugene, A.J., Nah, T., Tuet, W., et al., 2015. Secondary organic aerosol formation from the β-pinene + NO_3 system: effect of humidity and peroxy radical fate. Atmos. Chem. Phys. 15 (13), 7497–7522.
Chan, A., Chan, M., Surratt, J., Chhabra, P., Loza, C., Crounse, J., et al., 2010. Role of aldehyde chemistry and NO_x concentrations in secondary organic aerosol formation. Atmos. Chem. Phys. 10 (15), 7169–7188.
Chew, A.A., Atkinson, R., 1996. OH radical formation yields from the gas-phase reactions of O_3 with alkenes and monoterpenes. J. Geophys. Res. Atmos. 101 (D22), 28649–28653.
Draper, D., Farmer, D., Desyaterik, Y., Fry, J., 2015. A qualitative comparison of secondary organic aerosol yields and composition from ozonolysis of monoterpenes at varying concentrations of NO_2. Atmos. Chem. Phys. 15 (21), 12267–12281.
Eddingsaas, N.C., Loza, C.L., Yee, L.D., Chan, M., Schilling, K.A., Chhabra, P.S., et al., 2012. α-Pinene photooxidation under controlled chemical conditions - Part 2: SOA yield and composition in low- and high-NO_x environments. Atmos. Chem. Phys. 12 (16), 7413–7427.
Erisman, J.W., 2021. How ammonia feeds and pollutes the world. Science 374 (6568), 685–686.
Friedman, B., Farmer, D.K., 2018. SOA and gas phase organic acid yields from the sequential photooxidation of seven monoterpenes. Atmos. Environ. 187, 335–345.
Frisch, M., Trucks, G., Schlegel, H., Scuseria, G., Robb, M., Cheeseman, J., et al., 2016. Gaussian 16. Gaussian. Inc., Wallingford, CT, USA.
Gu, B., Zhang, L., Van Dingenen, R., Vieno, M., Van Grinsven, H.J., Zhang, X., et al., 2021. Abating ammonia is more cost-effective than nitrogen oxides for mitigating PM2.5 air pollution. Science 374 (6568), 758–762.
Guenther, A., Jiang, X., Heald, C.L., Sakulyanontvittaya, T., Duhl, T., Emmons, L., et al., 2012. The model of emissions of gases and aerosols from nature version 2.1 (MEGAN2. 1): an extended and updated framework for modeling biogenic emissions. Geosci. Model Dev. (GMD) 5 (6), 1471–1492.
Hand, J., Schichtel, B., Malm, W., Copeland, S., Molenar, J., Frank, N., et al., 2014. Widespread reductions in haze across the United States from the early 1990s through 2011. Atmos. Environ. 94, 671–679.
Hao, L., Kari, E., Leskinen, A., Worsnop, D.R., Virtanen, A., 2020. Direct contribution of ammonia to α-pinene secondary organic aerosol formation. Atmos. Chem. Phys. 20 (22), 14393–14405.
Hasan, G., Salo, V.-T., Valiev, R.R., Kubecka, J., Kurten, T., 2020. Comparing reaction routes for 3 (RO··· OR') intermediates formed in peroxy radical self-and cross-reactions. J. Phys. Chem. A 124 (40), 8305–8320.
Hoffmann, T., Odum, J.R., Bowman, F., Collins, D., Klockow, D., Flagan, R.C., et al., 1997. Formation of organic aerosols from the oxidation of biogenic hydrocarbons. J. Atmos. Chem. 26, 189–222.
Hopke, P.K., Querol, X., 2022. Is improved vehicular NO_x control leading to increased urban NH_3 emissions? Environ. Sci. Technol. 56 (17), 11926–11927.
Huang, R.-J., Zhang, Y., Bozzetti, C., Ho, K.-F., Cao, J.-J., Han, Y., et al., 2014. High secondary aerosol contribution to particulate pollution during haze events in China. Nature 514 (7521), 218–222.
Iinuma, Y., Böge, O., Gnauk, T., Herrmann, H., 2004. Aerosol-chamber study of the α-pinene/O_3 reaction: influence of particle acidity on aerosol yields and products. Atmos. Environ. 38 (5), 761–773.
Iyer, S., Rissanen, M.P., Valiev, R., Barua, S., Krechmer, J.E., Thornton, J., et al., 2021. Molecular mechanism for rapid autoxidation in α-pinene ozonolysis. Nat. Commun. 12 (1), 878.
Jia, L., Xu, Y., 2020. The role of functional groups in the understanding of secondary organic aerosol formation mechanism from alpha-pinene. Sci. Total Environ. 738, 139831.
Jimenez, J.L., Canagaratna, M., Donahue, N., Prevot, A., Zhang, Q., Kroll, J.H., et al., 2009. Evolution of organic aerosols in the atmosphere. Science 326 (5959), 1525–1529.
Kahnt, A., Vermeylen, R., Iinuma, Y., Safi Shalamzari, M., Maenhaut, W., Claeys, M., 2018. High-molecular-weight esters in α-pinene ozonolysis secondary organic aerosol: structural characterization and mechanistic proposal for their formation from highly oxygenated molecules. Atmos. Chem. Phys. 18 (11), 8453–8467.
Kenseth, C.M., Hafeman, N.J., Rezgui, S.P., Chen, J., Huang, Y., Dalleska, N.F., et al., 2023. Particle-phase accretion forms dimer esters in pinene secondary organic aerosol. Science 382 (6672), 787–792.
Kristensen, K., Jensen, L., Glasius, M., Bilde, M., 2017. The effect of sub-zero temperature on the formation and composition of secondary organic aerosol from ozonolysis of alpha-pinene. Environ. Sci.- Proc. Imp. 19 (10), 1220–1234.
Kumar, M., Li, H., Zhang, X., Zeng, X.C., Francisco, J.S., 2018. Nitric acid-amine chemistry in the gas phase and at the air-water interface. J. Am. Chem. Soc. 140 (20), 6456–6466.
Lelieveld, J., Evans, J.S., Fnais, M., Giannadaki, D., Pozzer, A., 2015. The contribution of outdoor air pollution sources to premature mortality on a global scale. Nature 525 (7569), 367–371.
Li, Y., Schichtel, B.A., Walker, J.T., Schwede, D.B., Chen, X., Lehmann, C.M., et al., 2016. Increasing importance of deposition of reduced nitrogen in the United States. Proc. Natl. Acad. Sci. U.S.A. 113 (21), 5874–5879.
Liu, C., Shi, K., 2021. A review on methodology in O_3-NO_x-VOC sensitivity study. Environ. Pollut. 291, 118249.
Liu, Y., Liggio, J., Staebler, R., Li, S.M., 2015. Reactive uptake of ammonia to secondary organic aerosols: kinetics of organonitrogen formation. Atmos. Chem. Phys. 15 (23), 13569–13584.
McCurdy, P.R., Hess, W.P., Xantheas, S.S., 2002. Nitric acid-water complexes: theoretical calculations and comparison to experiment. J. Phys. Chem. A 106 (33), 7628–7635.
Na, K., Song, C., Switzer, C., Cocker III, D.R., 2007. Effect of ammonia on secondary organic aerosol formation from α-pinene ozonolysis in dry and humid conditions. Environ. Sci. Technol. 41 (17), 6096–6102.
Ng, N.L., Chhabra, P.S., Chan, A.W.H., Surratt, J.D., Kroll, J.H., Kwan, A.J., et al., 2007. Effect of NO_x level on secondary organic aerosol (SOA) formation from the photooxidation of terpenes. Atmos. Chem. Phys. 7 (19), 5159–5174.
Nie, W., Yan, C., Yang, L., Roldin, P., Liu, Y., Vogel, A.L., et al., 2023. NO at low concentration can enhance the formation of highly oxygenated biogenic molecules in the atmosphere. Nat. Commun. 14 (1), 3347.
Nihill, K.J., Ye, Q., Majluf, F., Krechmer, J.E., Canagaratna, M.R., Kroll, J.H., 2021. Influence of the NO/NO_2 ratio on oxidation product distributions under high-NO conditions. Environ. Sci. Technol. 55 (10), 6594–6601.
Ohara, T., Akimoto, H., Kurokawa, J.-i., Horii, N., Yamaji, K., Yan, X., et al., 2007. An Asian emission inventory of anthropogenic emission sources for the period 1980–2020. Atmos. Chem. Phys. 7 (16), 4419–4444.
Orlando, J.J., Tyndall, G.S., 2012. Laboratory studies of organic peroxy radical chemistry: an overview with emphasis on recent issues of atmospheric significance. Chem. Soc. Rev. 41 (19), 6294–6317.
Paciga, A.L., Riipinen, I., Pandis, S.N., 2014. Effect of ammonia on the volatility of organic diacids. Environ. Sci. Technol. 48 (23), 13769–13775.
Park, J.-H., Babar, Z.B., Baek, S.J., Kim, H.S., Lim, H.-J., 2017. Effects of NO_x on the molecular composition of secondary organic aerosol formed by the ozonolysis and photooxidation of α-pinene. Atmos. Environ. 166, 263–275.
Pathak, R.K., Stanier, C.O., Donahue, N.M., Pandis, S.N., 2007. Ozonolysis of α-pinene at atmospherically relevant concentrations: temperature dependence of aerosol mass fractions (yields). J. Geophys. Res. Atmos. 112 (D3), D03201.
Perakyla, O., Berndt, T., Franzon, L., Hasan, G., Meder, M., Valiev, R.R., et al., 2023. Large gas-phase source of esters and other accretion products in the atmosphere. J. Am. Chem. Soc. 145 (14), 7780–7790.
Pullinen, I., Schmitt, S., Kang, S., Sarrafzadeh, M., Schlag, P., Andres, S., et al., 2020. Impact of NO_x on secondary organic aerosol (SOA) formation from α-pinene and

β-pinene photooxidation: the role of highly oxygenated organic nitrates. Atmos. Chem. Phys. 20 (17), 10125–10147.
Pye, H.O., Luecken, D.J., Xu, L., Boyd, C.M., Ng, N.L., Baker, K.R., et al., 2015. Modeling the current and future roles of particulate organic nitrates in the southeastern United States. Environ. Sci. Technol. 49 (24), 14195–14203.
Pye, H.O.T., Chan, A.W.H., Barkley, M.P., Seinfeld, J.H., 2010. Global modeling of organic aerosol: the importance of reactive nitrogen (NO_x and NO_3). Atmos. Chem. Phys. 10 (22), 11261–11276.
Reche, C., Perez, N., Alastuey, A., Cots, N., Pérez, E., Querol, X., 2022. 2011–2020 trends of urban and regional ammonia in and around Barcelona, NE Spain. Chemosphere 304, 135347.
Rissanen, M.P., 2018. NO_2 suppression of autoxidation-inhibition of gas-phase highly oxidized dimer product formation. ACS Earth Space Chem. 2 (11), 1211–1219.
Ronald, J.v.d.A., Mijling, B., Ding, J., Koukouli, M.E., Liu, F., Li, Q., et al., 2017. Cleaning up the air: effectiveness of air quality policy for SO_2 and NO_x emissions in China. Atmos. Chem. Phys. 17 (3), 1775–1789.
Sarrafzadeh, M., Wildt, J., Pullinen, I., Springer, M., Kleist, E., Tillmann, R., et al., 2016. Impact of NO_x and OH on secondary organic aerosol formation from β-pinene photooxidation. Atmos. Chem. Phys. 16 (17), 11237–11248.
Sekimoto, K., Fukuyama, D., Inomata, S., 2020. Accurate identification of dimers from α-pinene oxidation using high-resolution collision-induced dissociation mass spectrometry. J. Mass Spectrom. 55 (6), e4508.
Simon, M., Dada, L., Heinritzi, M., Scholz, W., Stolzenburg, D., Fischer, L., et al., 2020. Molecular understanding of new-particle formation from α-pinene between -50 and +25°C. Atmos. Chem. Phys. 20 (15), 9183–9207.
Sindelarova, K., Granier, C., Bouarar, I., Guenther, A., Tilmes, S., Stavrakou, T., et al., 2014. Global data set of biogenic VOC emissions calculated by the MEGAN model over the last 30 years. Atmos. Chem. Phys. 14 (17), 9317–9341.
Sobota, D.J., Compton, J.E., McCrackin, M.L., Singh, S., 2015. Cost of reactive nitrogen release from human activities to the environment in the United States. Environ. Res. Lett. 10 (2), 025006.
Stirnweis, L., Marcolli, C., Dommen, J., Barmet, P., Frege, C., Platt, S.M., et al., 2017. Assessing the influence of NO_x concentrations and relative humidity on secondary organic aerosol yields from α-pinene photo-oxidation through smog chamber experiments and modelling calculations. Atmos. Chem. Phys. 17 (8), 5035–5061.
Sutton, M.A., Oenema, O., Erisman, J.W., Leip, A., van Grinsven, H., Winiwarter, W., 2011. Too much of a good thing. Nature 472 (7342), 159–161.
Tao, F.M., 1998. Gas phase proton transfer reaction of nitric acid ammonia and the role of water. J. Chem. Phys. 108 (1), 193–202.
Tsiligiannis, E., Hammes, J., Salvador, C.M., Mentel, T.F., Hallquist, M., 2019. Effect of NO_x on 1,3,5-trimethylbenzene (TMB) oxidation product distribution and particle formation. Atmos. Chem. Phys. 19 (23), 15073–15086.
Wang, M., Kong, W., Marten, R., He, X.-C., Chen, D., Pfeifer, J., et al., 2020. Rapid growth of new atmospheric particles by nitric acid and ammonia condensation. Nature 581 (7807), 184.
Wildt, J., Mentel, T.F., Kiendler-Scharr, A., Hoffmann, T., Andres, S., Ehn, M., et al., 2014. Suppression of new particle formation from monoterpene oxidation by NO. Atmos. Chem. Phys. 14 (6), 2789–2804.
Yee, L.D., Isaacman-VanWertz, G., Wernis, R.A., Kreisberg, N.M., Glasius, M., Riva, M., et al., 2020. Natural and anthropogenically influenced isoprene oxidation in southeastern United States and central Amazon. Environ. Sci. Technol. 54 (10), 5980–5991.
Yu, Y., Ezell, M.J., Zelenyuk, A., Imre, D., Alexander, L., Ortega, J., et al., 2008. Photooxidation of α-pinene at high relative humidity in the presence of increasing concentrations of NO_x. Atmos. Environ. 42 (20), 5044–5060.
Zang, X., Zhang, Z., Zhao, Y., Li, G., Xie, H., Zhang, W., et al., 2024. Effects of NO_2 and SO_2 on the secondary organic aerosol formation from beta-pinene photooxidation. J. Environ. Sci. 136, 151–160.
Zang, X., Zhang, Z., Jiang, S., Zhao, Y., Wang, T., Wang, C., et al., 2022. Aerosol mass spectrometry of neutral species based on a tunable vacuum ultraviolet free electron laser. Phys. Chem. Chem. Phys. 24 (27), 16484–16492.
Zhang, P., Ma, P., Shu, J., Huang, J., Yang, B., Zhang, H., 2019. Characterization of crucial fragments during the nucleation and growth of secondary organic aerosol from the high-NO photo-oxidation of α-pinene. Atmos. Environ. 213, 47–54.
Zhang, X., McVay, R.C., Huang, D.D., Dalleska, N.F., Aumont, B., Flagan, R.C., et al., 2015. Formation and evolution of molecular products in α-pinene secondary organic aerosol. Proc. Natl. Acad. Sci. U.S.A. 112 (46), 14168–14173.
Zhang, Z., Zhao, Y., Zhao, Y., Zang, X., Xie, H., Yang, J., et al., 2024. Effects of NO and SO_2 on the secondary organic aerosol formation from isoprene photooxidation. Atmos. Environ. 318, 120248.
Zhao, D.F., Schmitt, S.H., Wang, M.J., Acir, I.H., Tillmann, R., Tan, Z.F., et al., 2018. Effects of NO_x and SO_2 on the secondary organic aerosol formation from photooxidation of alpha-pinene and limonene. Atmos. Chem. Phys. 18 (3), 1611–1628.
Zhao, Z., Zhang, W., Alexander, T., Zhang, X., Martin, D.B.C., Zhang, H., 2021. Isolating α-pinene ozonolysis pathways reveals new insights into peroxy radical chemistry and secondary organic aerosol formation. Environ. Sci. Technol. 55 (10), 6700–6709.